The Measurement of Recoil Force for Small Caliber Arms

Allen Dominek

Abstract

There are a variety of techniques to measure the perceived force from small arms recoil. The key word in these techniques is "perceived". The work reported here is the measurement of the actual recoil force generated and compared to a LEM calculation. The measurement techniques used are the measurement of the small arms acceleration using MEMS and the compression of a spring for the determination of the maximum force generated. Additional recoil measurements were taken for a variety of muzzle brakes.

Keywords: recoil, acceleration measurement, LEM

1. Introduction

Recoil forces from rifle or shotgun firings are a natural occurrence due to the acceleration of bullets and gases. Quantifying the recoil force has several applications. One is to appreciate the effect the recoil has on the shooter. Another could be to classify the performance of muzzle brakes.

Quantifying the force can be done through measurements or numerical means. Achieving realistic recoil forces numerically can be a challenging task. Computational fluid dynamics (CFD) solvers exist to model the phenomena. The phenomena could consistent of modeling the whole process of burning the powder to accelerate the bullet down the barrel or just to model the plumb of a muzzle blast as the gas leaves the muzzle using initial boundary conditions of the generated gas at the muzzle. There are many references for various CFD approaches [1] -[10].

An alternate numerical approach to that of a CFD solution is to use a lumped element method (LEM) as referenced in [11, 12]. Such a solution provides an internal ballistics solution for the motion of the bullet and average bulk motion for the expanding gas. No LEM solution is known for the gas characteristics once the bullet leaves the muzzle to account for the recoil impact of a muzzle brake.

The remaining techniques left to quantify the recoil forces are experimental (measurements). Four basic techniques available are the use of a load cell, accelerometer, photography and spring extension.

There are many references using load cells [13, 14, 15]. Fixtures are commonly used to support the firearm to achieve consistent measurements.

Measurements can be performed with the firearm being held too but the results may not be consistent since the load cell has to be restrained. Having the load cell restrained by ones shoulder offers realistic recoil data for the "apparent" recoil load on the shooter. Using a fixture to hold the firearm also may not yield a "true" recoil measurement. Rifles may generate maximum recoil forces of 3000 to 4000 lbs within a millisecond. Many fixtures may flex resulting in inaccurate peak recoil forces and resonate long after the primary recoil force.

Accelerometers offer an alternative for the firearm recoil measurements. This measurement approach offers the potential of accurate data if the firearm is not restrained. These references [16, 17] use accelerometers to measure the acceleration the firearm experiences during recoil. The force is calculated from this basic physics relationship, $F = ma$ where a is the acceleration and m is the mass of the firearm. It is this technique which will be utilized in the study.

Another technique is to film the firearm with high speed photography during firing. Many low cost cameras are available to film at a frame rates 960 fps or at much higher frame rates with specialized cameras. An estimate of the firearm velocity can be acquired by monitoring the position of the firearm in each frame. The velocity is numerically obtained from the position vs time record. Acquiring acceleration data from positional data is also possible if sufficient accuracy in positional data could be obtained; however, this is generally not the case at these resolutions for this application. The positional accuracy from is not sufficient from pixel discretization to perform a 2nd order derivative to determine the acceleration.

The other technique employs the extension of a spring to measure the recoil force. The fixture would have the firearm or its receiver mounted to a platform with ball bearing glides. A spring would be attached between the platform and the rest of the fixture. A sensor could be used to monitor the position of the platform as a function of time, however, the inherit drag of ball bearing glides would inhibit any accurate measurement. This approach then would only provide a relative measurement of the maximum recoil of different firearms.

The calculations and measurements provided within are to study and examine the recoil forces with and without muzzle brakes using a Zastava LK M70 7 mm firearm and a Remington 7-08 cartridge. The measurement technique studied here involves a MEMS accelerometer and the measurements are compared to numerical results. Four different muzzle brakes are used with different geometry parameters to explore their impact on the recoil force. Naturally, the use of only four muzzle brakes does not provide sufficient data to make any generic claims on what the ideal geometry parameters should be to minimize the recoil force.

2. Analytical Relationships

The recoil that a firearm has (with or without a muzzle brake) can be acquired directly through measurements on the firearm or inferred indirectly from the motion of the bullet and gas. A common relationship relating the motion of an unrestrained firearm to the motion of the bullet and gas is

$$p_r = m_{gun} v_{gun} = m_b v_b + m_g v_g. \tag{1}$$

which enforces the conservation of momentum of the system and this relationship holds for any time value. p_r is the recoil momentum where the subscripts b and g refer to the bullet and gas, respectively. The recoil force can be determined by taking the derivative of the momentum which is

$$F_r(t) = \frac{dp_r}{dt} = m_b a_b + \frac{dm_g}{dt} v_g + m_g a_g \tag{2}$$

yielding

$$F_r(t) = F_b(t) + F_g(t) \tag{3}$$

where F_r is the recoil force of the firearm, F_b is the force of the bullet and F_g is the force of the gas. Note that there is a contribution to the force from the gas which involves the temporal derivative of its mass until all the powder has burnt.

There are a few figures of merits to characterize recoil. One is the force of the recoil. Another is the velocity of the recoil. A third is the impulse response of the recoil. The impulse response J of a force is given by

$$J = \int F_r dt \tag{4}$$

which is the integral of the force over time. The impulse response is related to an object's momentum and both have the same dimensions.

Note that the pressure at the base of the bullet can be inferred from the bullet's acceleration, a_b with these relationships

$$P = F_b/A = m_b * a_b/A \tag{5}$$

where P is the pressure on the bullet and A is the cross-sectional area of the bullet.

A number of sources provide expressions for firearm recoil velocity. These expressions are typically for when the bullet leaves the barrel. One reference for recoil velocity determination is from SAAMI [18] using Eq. 1. This reference provides suggested velocities for the gas relative to the muzzle velocity of the bullet and is shown in Table 1 where v_b is the bullet's muzzle velocity.

Another velocity estimate can be obtained by approximating the gas velocity distribution in the barrel as linear from the breach (0 ft/s) to the bullet's position (v_b) [19]. This results in the average gas velocity to be one-half of the bullet velocity. Note that this is substantially different from the guidance provided in Table 1 [18]. It is shown later with measurements that a factor of 1 provides excellent agreement between theory and measurement.

Table 1:
Muzzle gas velocities

Firearm	Gas velocity
High power rifles	$1.75v_b$
Shutguns (average length)	$1.5v_b$
Shutguns (long barrel)	$1.25v_b$
Pistol & revolvers	$1.5v_b$

3. Muzzle Brakes

There are many muzzle brakes available to reduce recoil and many articles and videos comparing their effectiveness. Most muzzle brakes have a cylindrical shape most likely due to ease of manufacture and cost. The number of ports varies for a muzzle brake but it is dependent upon the powder charge and bullet caliber for the firearm. In these measurements, the powder used was IMR 4350 with a load charge of 43.7 grains. The bullet used was a 162 grain Hornady ELD-Match bullet in a Remington 7-08 case. The measured muzzle velocity is 2550 ft/s for the configuration as measured with a chronograph.

Figure 1 illustrates four muzzle brakes used in this testing. Two have a rectangular cross-section and two have a cylindrical cross-section. The rectangular shaped muzzle brakes were made by the author. The cross-sectional shape was essentially 1"x2". MB1 was based upon a muzzle brake provided by [20]. MB3 was obtained from [21]. MB2 had essentially the same cross-section shape as MB1 but with the port dimensions of those in MB3. MB4 was obtained from an eBay site. The essential dimensional data for these muzzle brakes are provided in Table 2.

Table 2:
Muzzle brake parameters (inches)

Parameter	Port width	Port height	Port depth	Bore diameter
MB1	.596	.800	1.880	.319
MB2	.325	.775	1.980	.312
MB3	.340	.550	.826	.372
MB4	.390	.665	.980	.340

4. Lump Element Model

An internal ballistic solution for the bullet's velocity and bore pressure provides a reference solution for the firearm recoil force. This solution in-

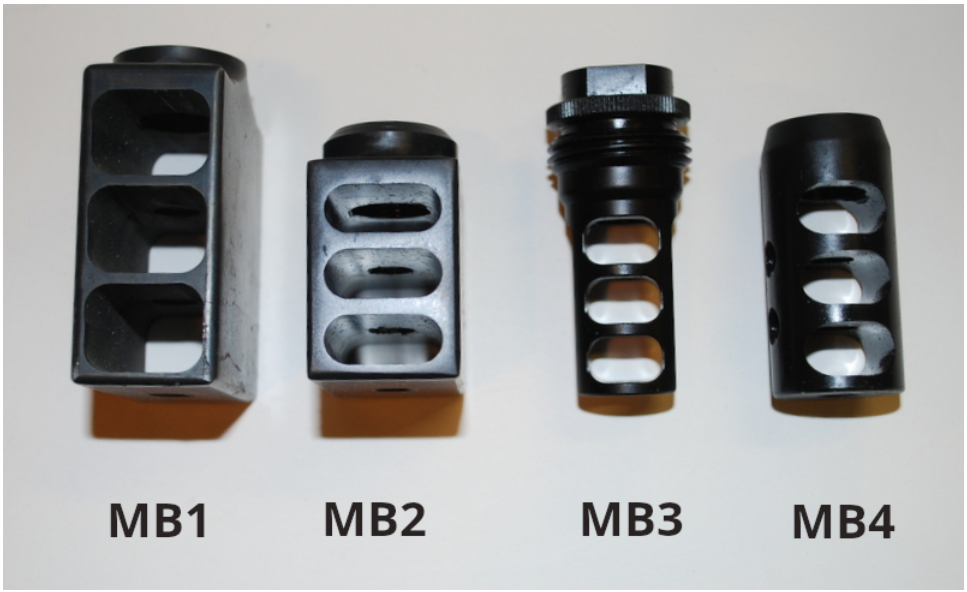

Figure 1: Illustration of the four, 3 ported muzzle brakes used.

volves solving for the bullet's velocity, pressure and the percentage of burnt powder as a function of time.

The equations of interest are:

$$\frac{dz}{dt} = \frac{\beta}{D_w} P^a \tag{6}$$

$$\frac{dx}{dt} = v \tag{7}$$

$$\frac{dv}{dt} = \frac{\pi r^2}{m_b} \left[P - P_{atm} - P_r \right] \tag{8}$$

where the unknowns are v, x and z which are the velocity of the bullet, the position of the bullet and the normalized amount of burnt powder as described in [11]. These equations are solved by a 4th order Runge-Kutta solver. Using the parameters in Table 3, the internal ballistic solution for the unknowns is shown in Figures 2 through 4. As noted earlier, 43.7 grains of IMR 4350 powder was used for a Rem 7-08 case with a 162 grain bullet. Note the discontinuity in the calculated pressure when all the powder is burnt suggests that the model has limitations. However, this model has matched the peak pressure and location for other tested loads when strain gauges where used for pressure determination.

Table 3:
Lumped method input data

Parameter	Value
Projectile radius, r	.0036068 m
Projectile mass, m_b	162 grns
Propellant mass, m_p	43.7 grns
Propellant density, ρ	1523 kg/m^3
Web thickness, D_w	4.4 10^{-4} m
Propellant burning rate constant, β	8.1525 10^{-7}m/s/Pa^{-a}
Propellant pressure index, a	.70150
Propellant impetus, F	1023.45 10^3 J/kg
Specific heat ratio, γ	1.22
Form function coefficient, k	0
Co-volume, c	.00089 m/kg
Primer energy, E_i	69 J
Pressure, resistance, P_r	5.9 10^6 Pa
Pressure, atmospheric, P_a	1.0 10^5 Pa
Case volume, V_c	3.1844 10^{-6} m^3
Barrel length, L	.5235 m

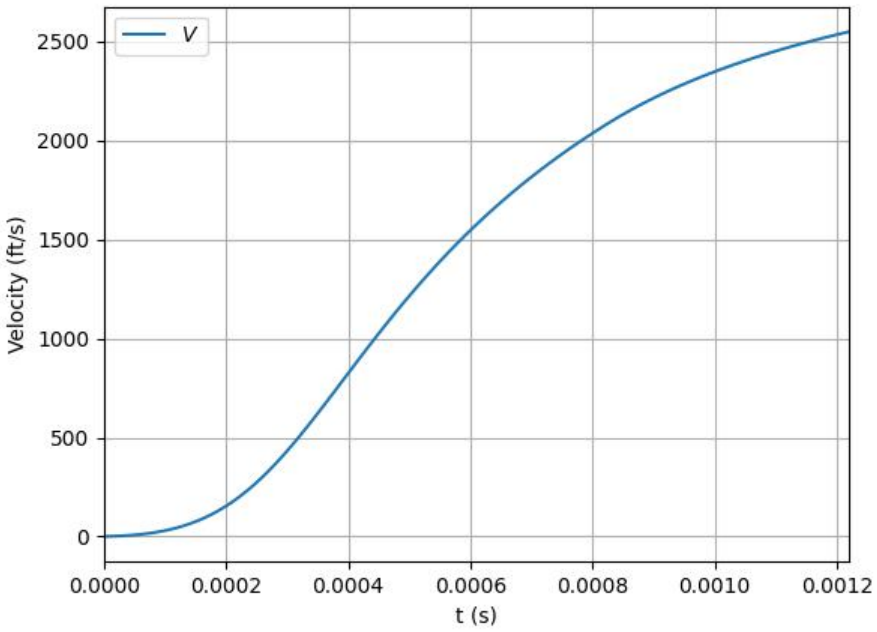

Figure 2: Calculated bullet velocity for the bullet in the barrel.

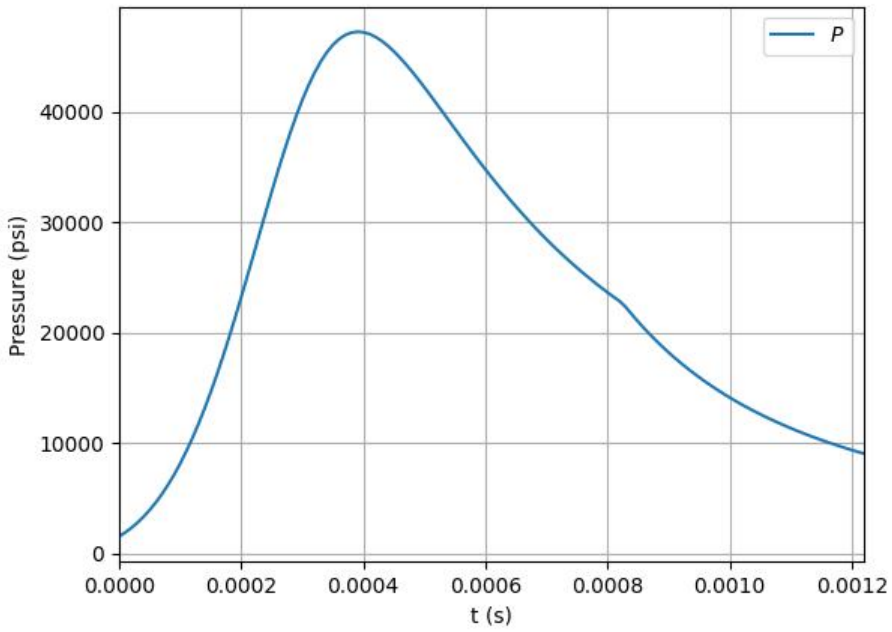

Figure 3: Calculated pressure on the bullet for the bullet in the barrel.

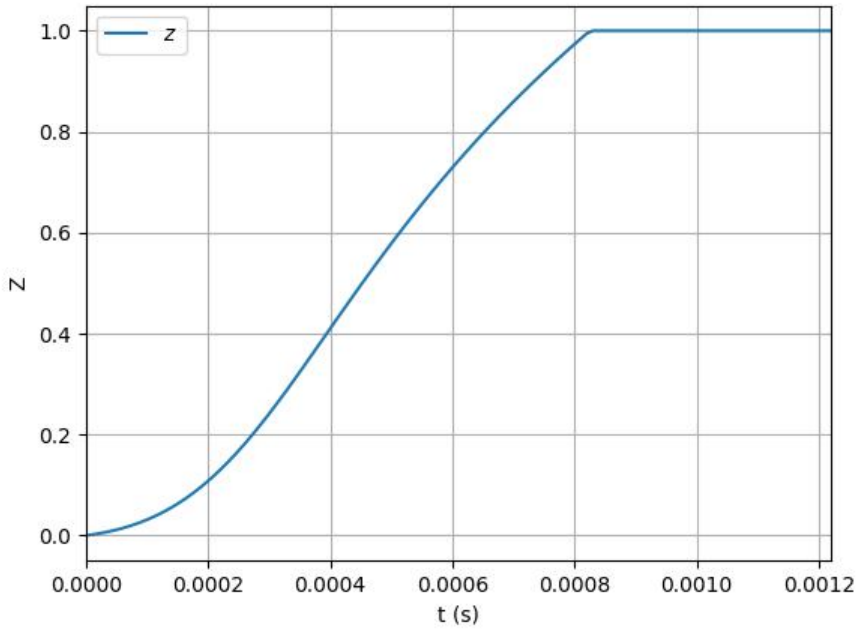

Figure 4: Calculated normalized burnt powder.

The resulting recoil force and impulse response due to the bullet and gas is shown in Figure 5 and was obtained by taking the time derivative of the momentum for the bullet and gas. The mass of the gas was determined by the initial mass of the powder times the calculated burnt powder ratio, $z(t)$. The gas velocity referenced in Equation 2, v_g is set to the bullet velocity, v_b. Validation of this velocity decision will be demonstrated later.

Note the shape discontinuity in the gas force contribution which is when the time derivative of the mass of the gas goes to zero. This could be an artifact from the LEM burn equation. Physical processes generally have a smooth and continuous change.

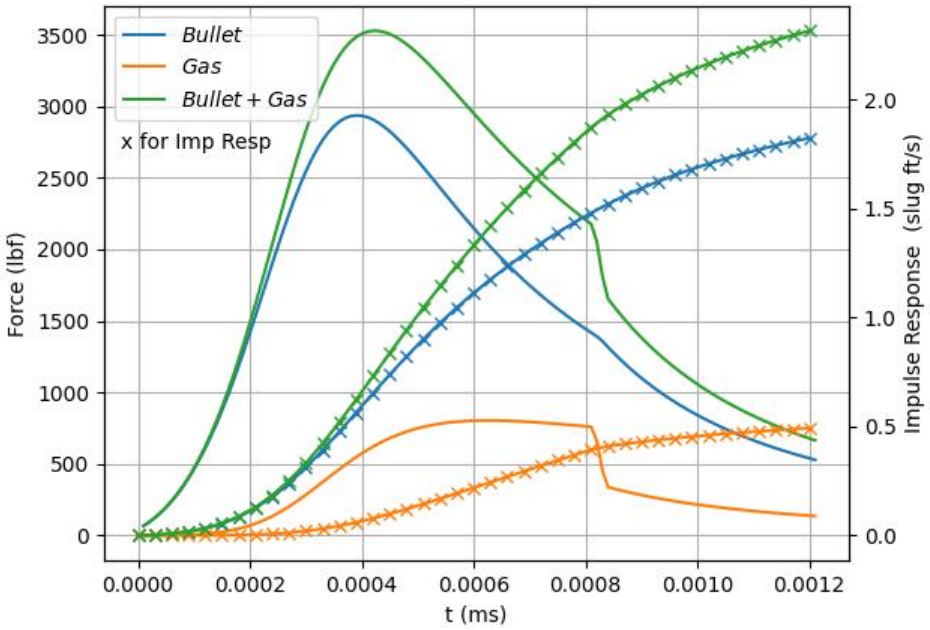

Figure 5: The calculated recoil force and impulse response due to the bullet and gas.

The recoil velocity of the firearm and its displacement can be calculated using the LEM results using Eq. 1 to obtain velocity and displacement is given by $v_{gun}t$. Figure 6 illustrates the firearm's recoil velocity and the amount of displacement an unrestricted firearm experiences while the bullet is within the barrel for firearm weight of 11.027 lbs. Eq. 1.

5. CFD Modeling

The impact of the muzzle brake was calculated for muzzle brake MB1 using OpenFOAM [22] and integrating the HiSA solver [23] with it. The FOI references [9], [10] have also used OpenFOAM for their ballistics simulations. The numerical model employed a quarter sphere for the calculation domain as shown in Figure 7. It used three different mesh densities for a total of 1269378

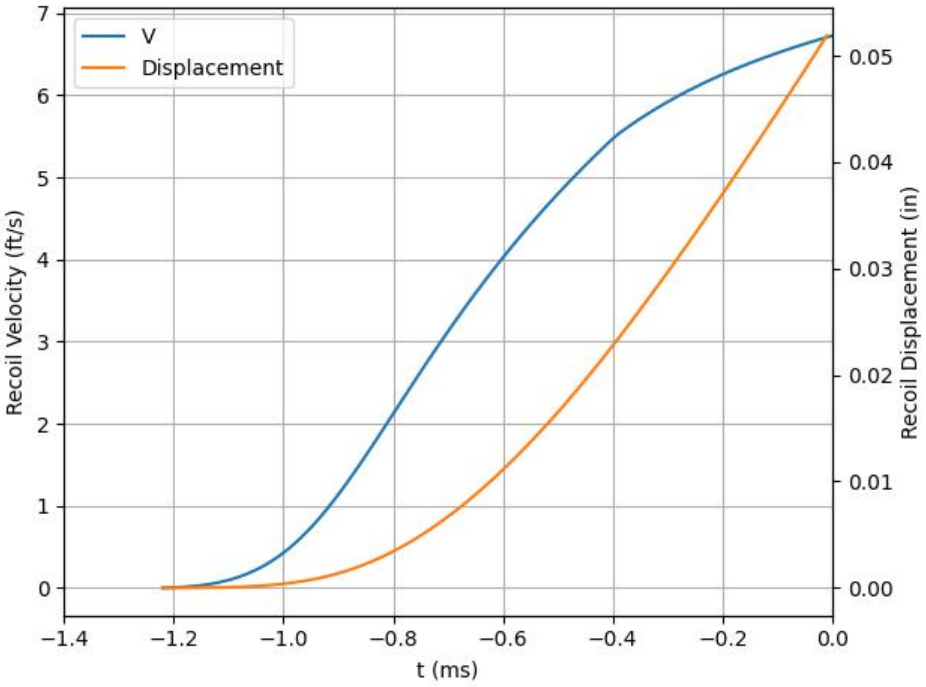

Figure 6: The firearm motion due to recoil from the bullet while the bullet is in the barrel for a firearm weight of 11.027 lbs.

cells. The mesh was generated by cfMESH from the CfdOF workbench of FreeCAD [24]. The workbench also generated the initial input files for the OpenFOAM simulation but these were edited for use with the HiSA solver.

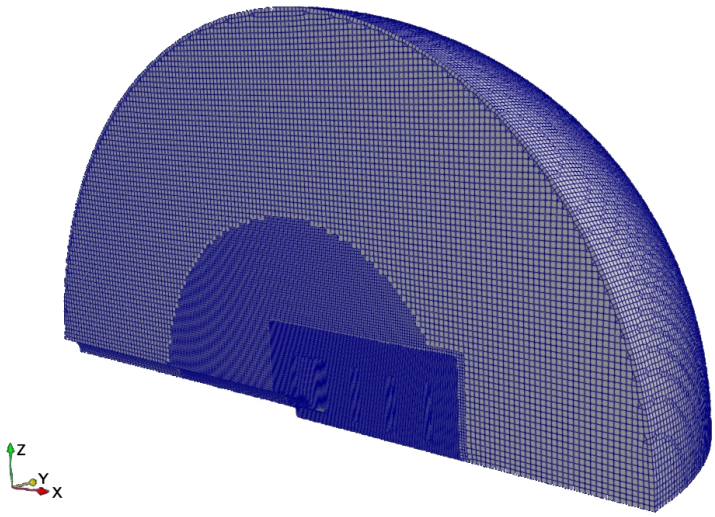

Figure 7: The meshed calculation domain for the CFD simulation.

The mesh had 5 boundary surfaces with each having a unique boundary condition. The boundary condition on the spherical surface was set to a far-field condition, the two planar surfaces were set to a symmetry condition, the metal surfaces were set to a no-slip condition and the surface representing the muzzle opening of the barrel was set to an inlet condition. The inlet boundary conditions are described later. Figure 8 illustrates the geometry and the location of the inlet/muzzle surface shown in red.

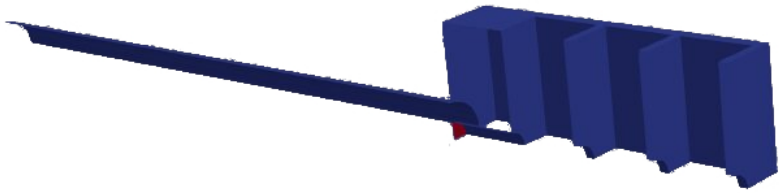

Figure 8: Illustration of the geometry and location of the inlet surface (shown in red).

The inlet boundary condition was based upon a blowdown model where gas is leaving an orifice from a reserve [12], [25]. The model provides time dependent values for the pressure, temperature and velocity at the muzzle where the flow is choked. Depending upon if the muzzle temperature is assumed constant during the derivation of the choked muzzle pressure dependency, there are two analytical forms possible for the blowdown model. The expression for a variable temperature has a power law form while the other expression has an exponential form. Considering the approximations, either form is suitable but the exponential form was used in this case. Table 4 provides the analytical representations of these forms describing the pressure, temperature and velocity temporal distributions.

Table 4:
Blowdown Model Forms

Quantity	Exponential	Power Law
$P(t)$	$P_0 e^{(-t/\tau_p)}$	$P_0(1+t/\tau_2)^{-2\gamma/(\gamma-1)}$
$T(t)$	$T_0 e^{(-t/\tau_t)}$	$T_0(1+t/\tau_2)^{-2}$
$U(t)$	$U_0 e^{(-t/\tau_u)}$	$U_0(1+t/\tau_2)^{-1}$

The initial values for these variables are

$$P_0 = P0 * (2/(\gamma + 1))^{\gamma/(\gamma-1)} \tag{9}$$

$$T_0 = T0 * 2/(\gamma + 1) \tag{10}$$

$$U_0 = \sqrt{\gamma R T0} \tag{11}$$

where $P0 = 85.42$ MPa and $T0 = 1800$ K are the initial pressure and temperature values of the muzzle gas with $\gamma = 1.245$. The specific gas constant R for the muzzle gas is given by $R = R_g/mol\_w$ $\mathrm{m}^2/\mathrm{s}^2/\mathrm{K}$. R_g is the general gas contant with a value of 8314 J/(K kmol) and mol_w is the molecular weight of the muzzle gas with an estimated value of 24.77 kg/kmol. The molecular weight of the muzzle gas was estimated from the gas distribution shown in Table 5.

Table 5:
Muzzle gas composition

Species	Mole fraction
CO_2	.44
H_20	.22
CO	.11
N_2	.12
H_2	.11

The τ values are given by

$$\tau_p = V/(BA\sqrt{\gamma T0}) \tag{12}$$

$$\tau_t = \gamma/(\gamma - 1) * \tau_p \tag{13}$$

$$\tau_u = 2\gamma/(\gamma - 1) * \tau_p \tag{14}$$

$$\tau_2 = 2\gamma/(\gamma - 1) * \tau_p \tag{15}$$

where $V = 2.333e^{-5}$ m^3 is the volume of the case and barrel, A is the cross sectional area of the barrel and B is given by

$$B = \sqrt{\gamma} * (2/(\gamma + 1))^{(\gamma+1)/(2(\gamma-1))}. \tag{16}$$

A lookup table was generated for each of the pressure, temperature and velocity variables for every 10 microseconds. Interpolation was used in OpenFOAM to acquire the required values from these tables. Additionally, the

calculation started at -30 microseconds in an attempt to simulate the muzzle gas leaking by the engraving as the bullet leaves the muzzle and to allow for greater numerical stability by not having OpenFOAM start with such a large impulsive initial boundary conditions at the geometry inlet. The numerical value for τ_p, as given by the expression shown in Eq. 12, is 1.18 10^{-3} ms. However, τ was emperically determined that this value should be approximately 1.4 10^{-3} ms.

Two turbulence models were used, a RANS (Reynolds-Averaged Navier-Stokes) using kOmegaSST and LES (Large Eddy Simulation) using Smagorinsky modeling. Both had similar generated forces due to the pressures in the ports. Each used a time step of .1 microsecond and 4 milliseconds of simulation were calculated. The HiSA solver used an implicit two stage time-stepping method. The simulations were performed on an AMD Ryzen 9 7950X3D processor using 14 of its 16 cores.

The calculation pressures in the ports along three lines located at 7 mm, 14 mm and 21 mm above the bore's center line are shown in Figure 9 at $t = .06$ ms which correspond to when the closest port has the largest pressures. The center line of the barrel is directed along the x-axis and the ports openings are in the z direction. As can be seen, the port farthest from the muzzle had little impact on the reducing recoil force. The width of the muzzle brake could also be reduced. There was little benefit, as shown at $z = 21$ mm location, since the pressure distribution was constant. The calculated x-directed forces and the impulse responses for the muzzle brake are shown in Figure 10.

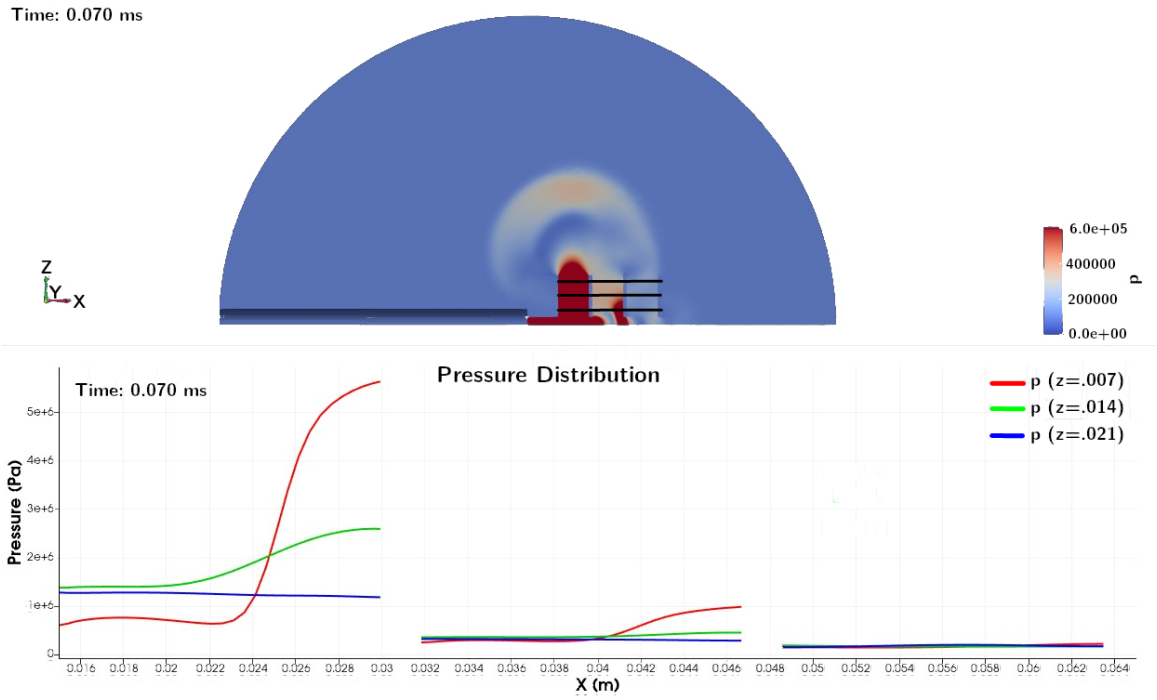

Figure 9: Calculated pressures for MB1.

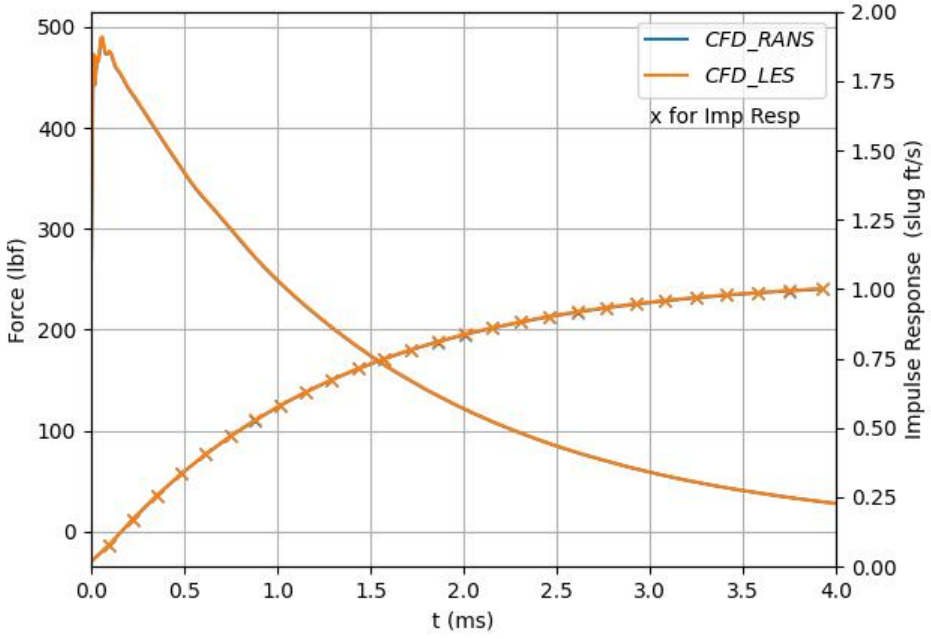

Figure 10: Calculated muzzle brake forces and impulse responses using RANS and LES for MB1. The results barely differ.

6. Accelerometer Measurements

Accelerometer measurements were taken to better capture the recoil effects and characterizing recoil effects from a muzzle brake. Measuring the acceleration as a function of time permits the determination of the firearm recoil force, velocity and position. An Analog Devices MEMs accelerometer ADXL1004 was used in these measurements. It can measure accelerations up to 500 g ($1g = 9.81 m/s^2$). The output signal of the accelerometer is a voltage proportional to the acceleration. The calibration scale factor is 4 mV/g. The voltage was measured with a Tektronix MDO3104 oscilloscope. The observed trace was referenced and recorded when the bullet exited the barrel as described earlier. The accelerometer was mounted to the firearm's rail as shown in Figure 11.

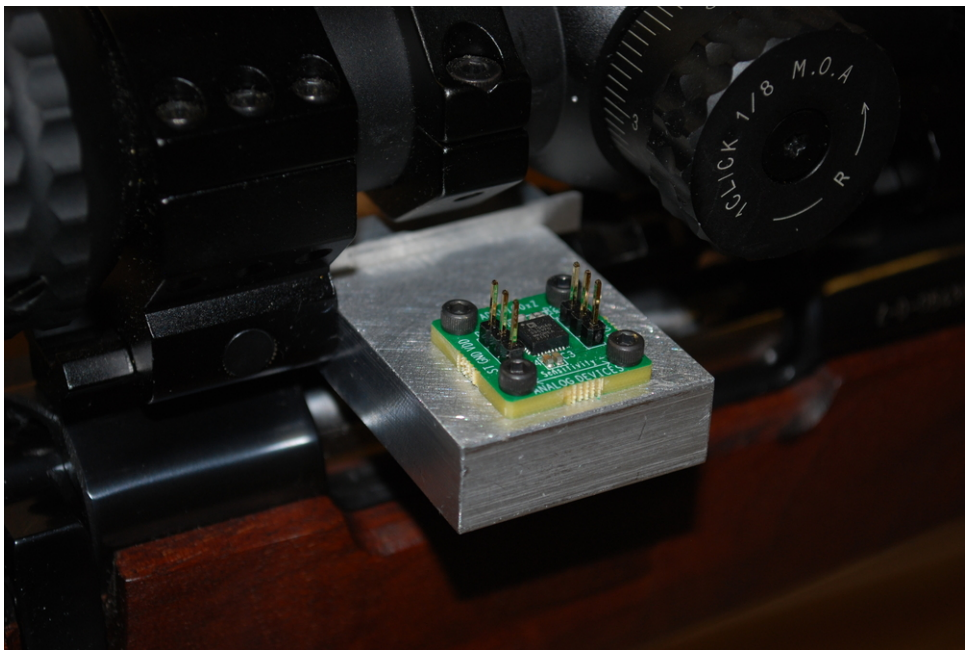

Figure 11: Accelerometer mounted to firearm.

The measurement configuration consisted of suspending the receiver using a 1/16" OD diameter wire rope as shown in Figure 12. This configuration offers minimal mounting drag for recoil measurements and good repeatability. The weight for the receiver, mounting hardware and trigger actuator was 11.027 lbs. The FOI references [9, 10] also used a pendulum configuration but its construction may have limited its sensitivity. The trigger release was achieved through the use a 12 V linear actuator as shown in Figure 13.

Figure 14 illustrates a typical measured result. The oscilloscope trigger ($t = 0$) occurs when the bullet exits the barrel. The measured result has significant high frequency variations in the waveform. Transforming the time domain waveform into the frequency domain using a FFT results in the spectral content shown in Figure 15. Aside from general broadband

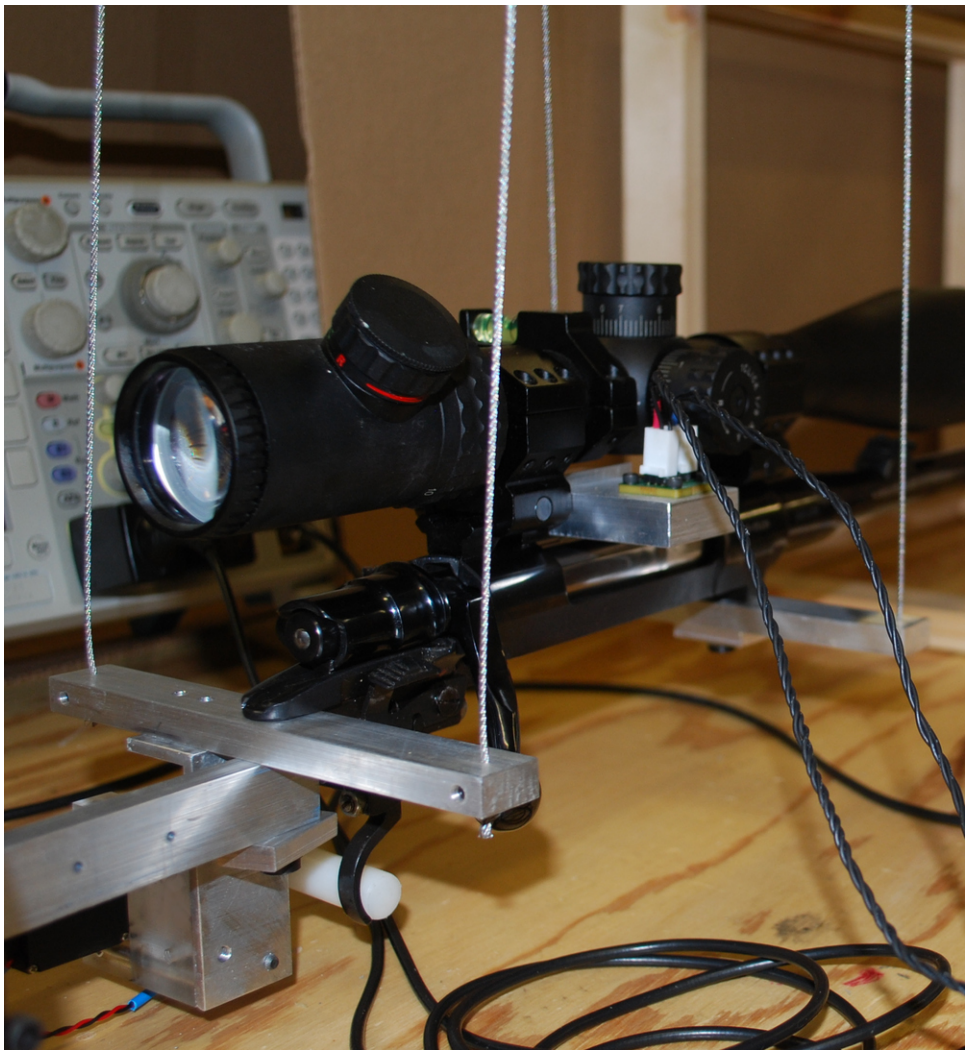

Figure 12: Illustration of firearm pendulum mounting configuration.

noise, there are sources of localized spectral contributions. One of them occurs around 45 MHz which is due to an internal resonance of the MEMS accelerometer. There are other lower frequency spectral contributions, too. The spectral content above 2 kHz appears not to be very significant for the velocity and displacement information since those curves are fairly invariant if higher spectral information is included or not. Figure 16 illustrates the original and filtered waveforms.

Acceleration measurements were taken for the bare muzzle and four muzzle brakes. These measurements were processed to obtain the recoil velocity and displacement as a function of time. The velocity data was obtained by integrating the acceleration data (no low pass filtering) and the displacement data was obtained by integrating the velocity data. Figures 17 and 18 illustrate the integrated data for the pendulum configuration using the wire rope. The velocity data is proportional to the impulse response of the recoil

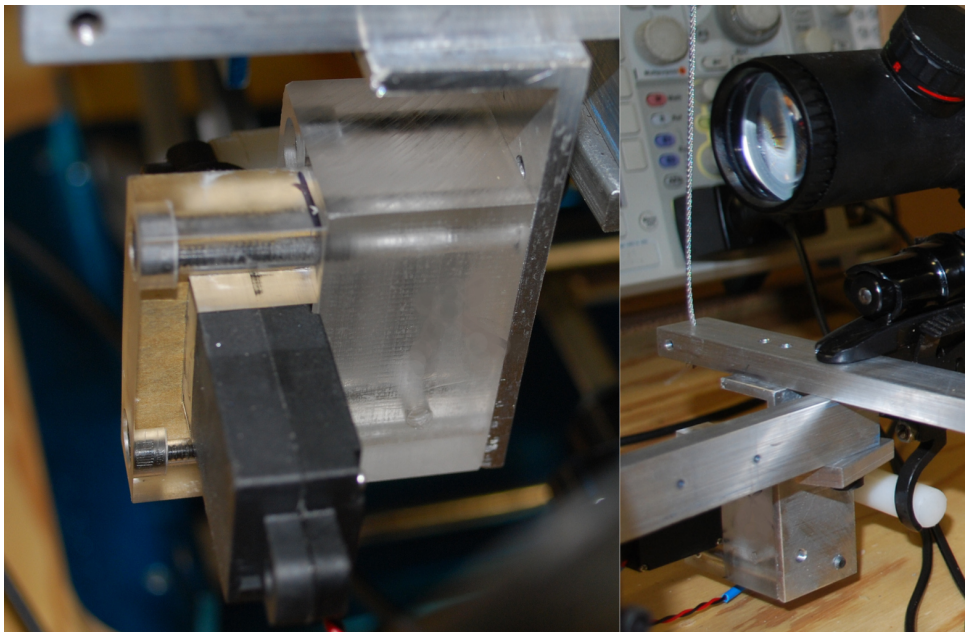

Figure 13: Illustration of trigger actuator used.

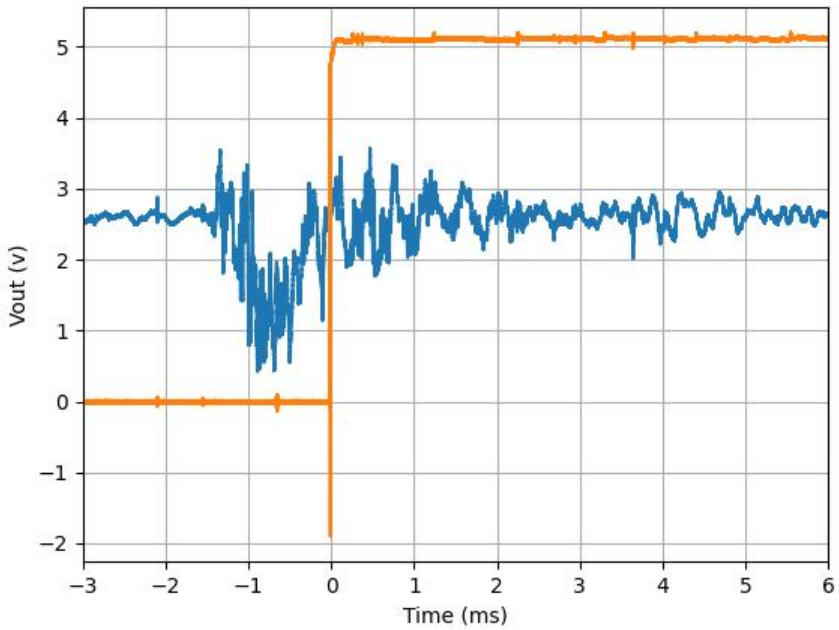

Figure 14: Illustration of a typical measured waveform and the trigger signal.

process. The displacement data provides an indication of acceleration and velocity changes during the recoil process. The pendulum fixture has minimal drag and is conducive to more sensitive/accurate acceleration measurements than other fixtures.

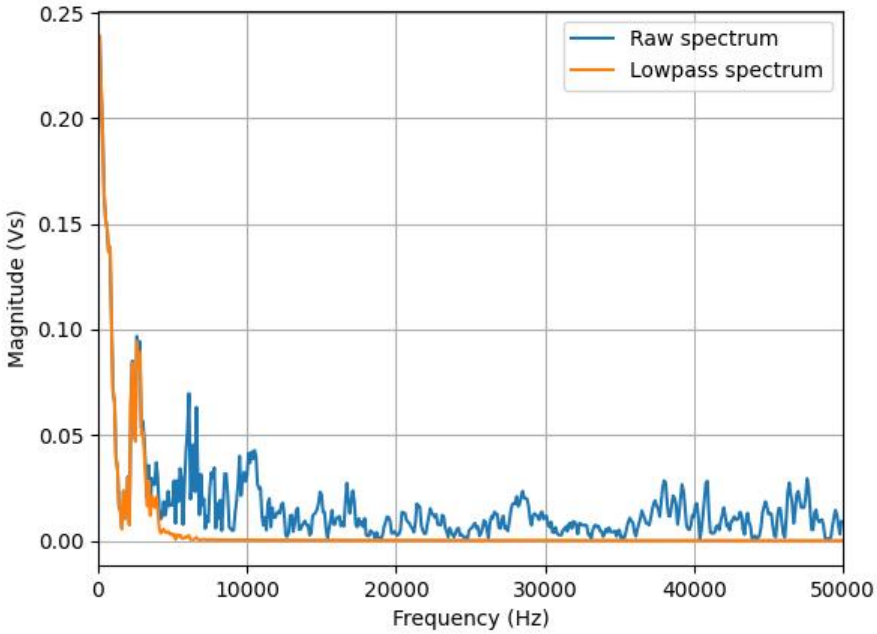

Figure 15: Spectral content of a typical measurement and its filtered spectrum.

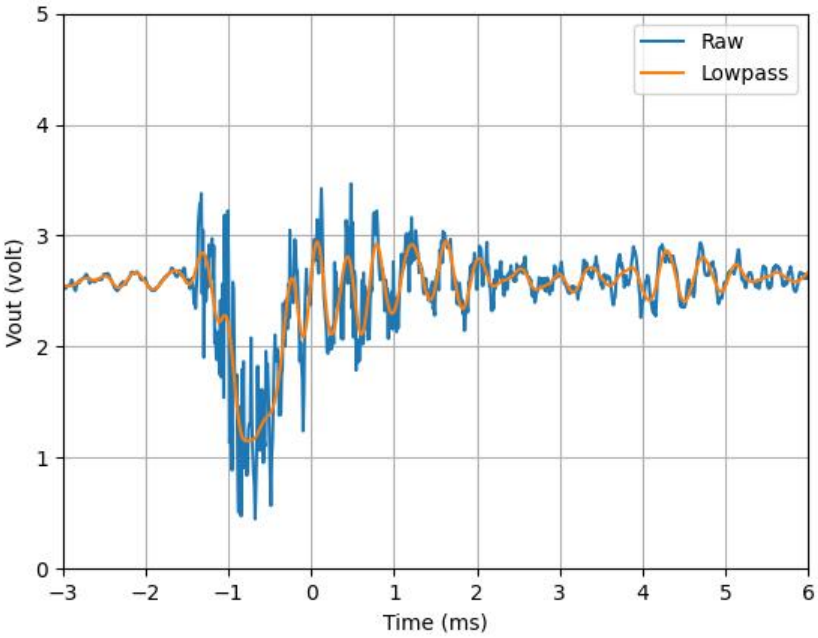

Figure 16: Comparison of unfiltered and filtered waveforms.

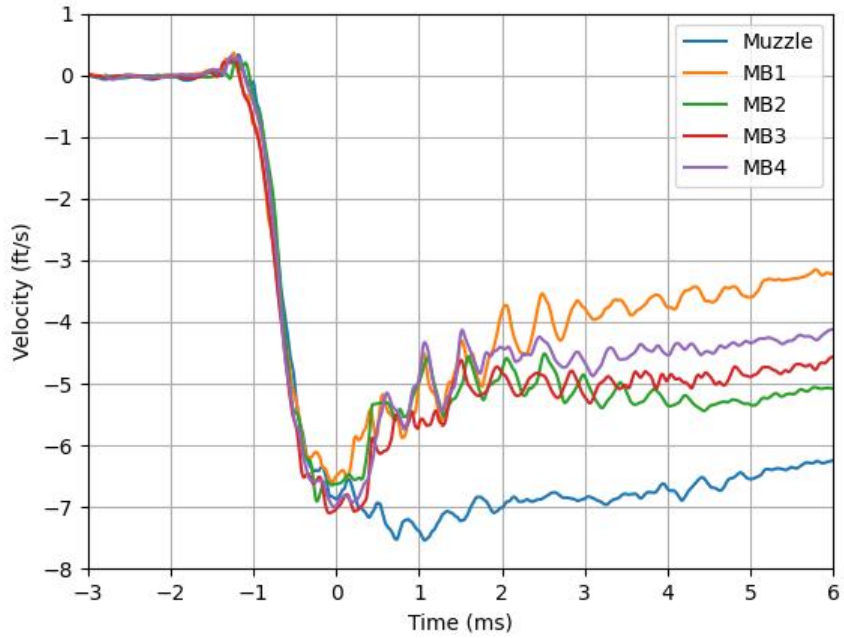

Figure 17: Firearm recoil velocities for the various muzzle brakes with the pendulum configuration.

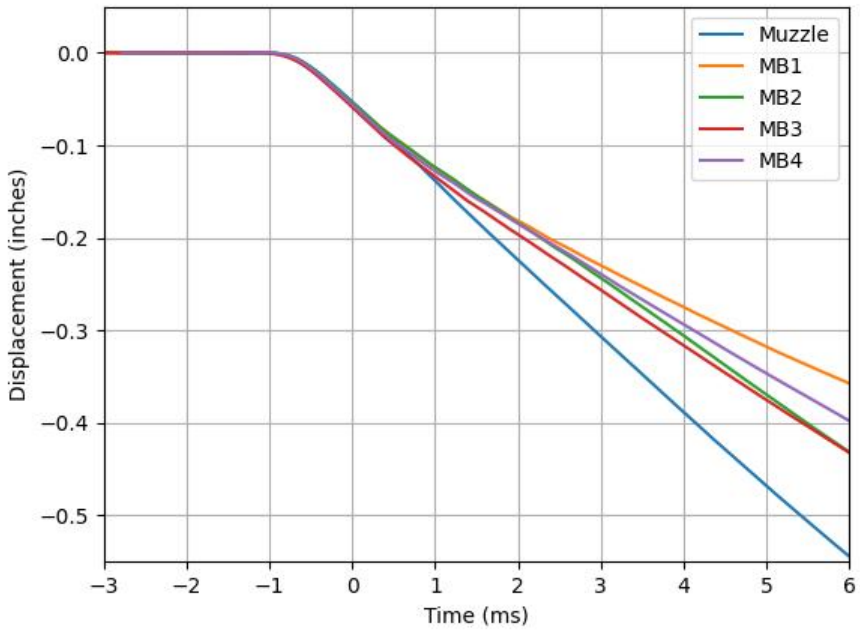

Figure 18: Firearm recoil displacement for the various muzzle brakes with the pendulum configuration.

Note that the maximum velocity for each muzzle termination is essentially the same regardless of the muzzle condition (no muzzle brake or with muzzle brake) at t=0 s. This suggests whatever gas leaks around the bullet as it travels down the barrel, it is insufficient to have a noticeable interaction with the muzzle brake. In all cases, the dominant recoil acceleration stops after $t = 0$ s which is when the bullet exits the barrel. The major impact of the muzzle brakes occurs after $t = 0$ s.

The acceleration the pendulum configuration experienced with the no muzzle brake and the MB1 muzzle brake is shown in Figure 19. Notice that the acceleration before the bullet's barrel exit is consistent between the two measurements. After $t = 0$ s, there is reverberation which becomes more pronounced with the presence of the muzzle brake. It is believed these reverberations are due to a gas pulse wave traveling along the barrel. The periodicity is .5 ms and the barrel length is $1.7'$ so the velocity is 6800 ft/s which is conceivable for a compressed gas. These reverberations are barely present in the no muzzle brake case and present in all the muzzle brake cases. The data in this plot was processed with a 4th order low-pass filter with a cutoff frequency of 4 kHz. The harmonic frequency of these reverberations is 2 kHz.

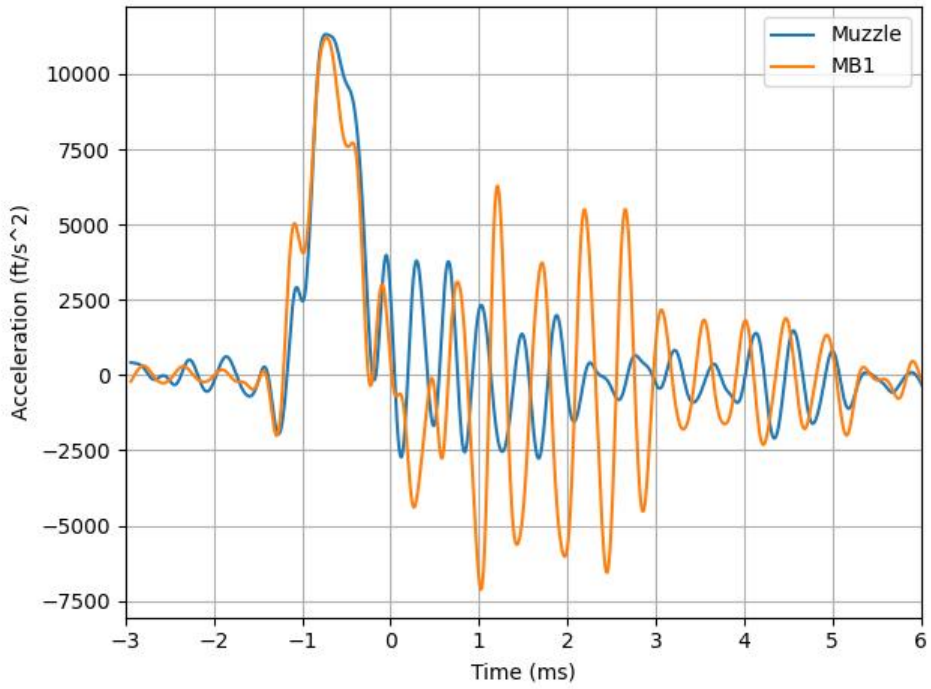

Figure 19: Measured acceleration for the firearm with a muzzle brake and the MB1 muzzle brake.

Figure 20 illustrates a comparison between the impulse response for the firearm obtained from the measured acceleration and the calculated impulse responses for the bullet and gas obtained by the LEM calculations for the

pendulum measurement configurations. Excellent agreement exists between the measurement and calculations. The bullet's impulse response was calculated with the velocity shown in Figure 2 for the no muzzle brake cases. The gas's impulse response was calculated with the bullet velocity multiplied by 1.0 for the gas velocity with the gas mass calculated by the powder mass times the normalized burnt powder shown in Figure 4. The use of a velocity factor of 1.75 would not have provided a result that would have matched the measurement. Neither would have using a model that the average velocity of the gas column is one-half of the bullet's velocity.

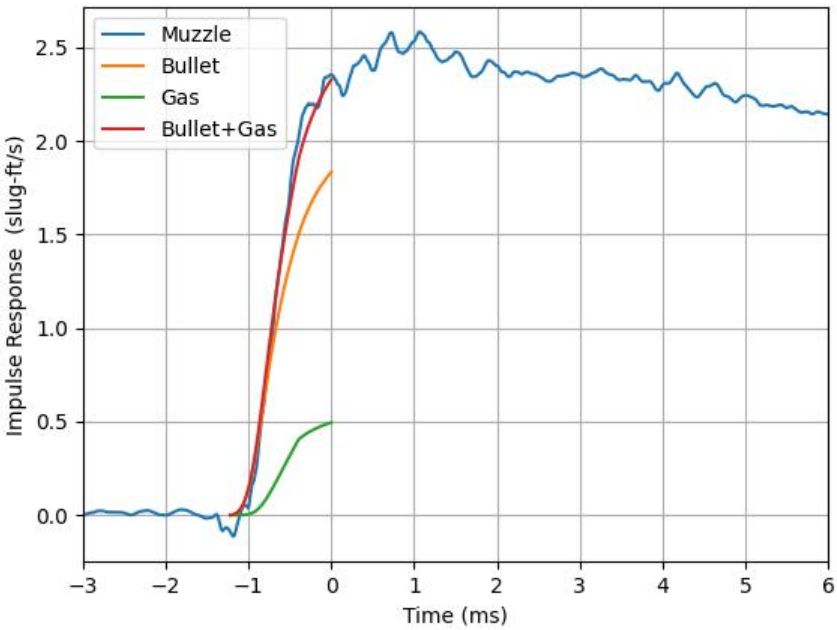

Figure 20: Firearm impulse (measured) compared with the bullet and gas impulse response (LEM calculation) with the pendulum configuration.

Figure 21 compares the measured impulse response from the pendulum fixture to the LEM calculated impulse response from the bullet and gas which created the recoil force and the restraining CFD calculated impulse responses for the MB1 muzzle brake. Note the presence of the reverberations in the impulse response past $t = 0$ s due to the gas pulse wave in the barrel. The calculated internal ballistics and CFD responses provide results which matches reasonable well with the measured results.

7. Conclusions

Firearm recoil measurements were taken to rigorously examine bullet and gas contributions solely due to the recoil. Previous force measurements included the "system response" of holding the firearm by a person or the fixture

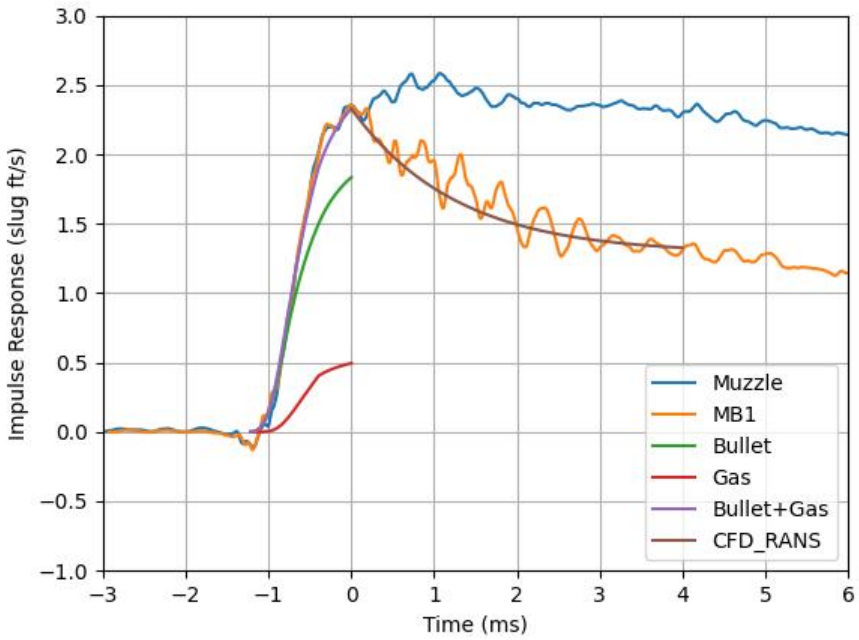

Figure 21: Firearm impulse response (measured) compared with the bullet, gas and muzzle brake (MB1) impulse response (calculated) with the pendulum configuration.

restraining the firearm. This resulted in a very long response time with late time reverberations. The sampling rate for these prior measurements then did not require a very fast sampling rate since the system response time was very large compared to the measurements made here.

It was demonstrated that a simple one-dimensional LEM predicted the recoil behavior of a firearm when the bullet is in the barrel. Once the bullet left the barrel, a more complex CFD model was used to calculate the restoring force from a muzzle brake which compared well to measurements too.

The use of a MEMS acceleration sensor, temporal measurements can be made to study the internal ballistics of a firearm and the impact of muzzle brakes.

Acknowledgements

The author would like to thank Sean Gilmore for his interest in this topic and reviewing the manuscript.

References

[1] Lei, H., Wang, Z. and Zhao, J., "Stress Analysis of Muzzle Brake by Using Fluid-Solid Coupling Method", *Journal of Engineering Science and Technology Review*, Sept. 4, 2016, pp. 48-55.

[2] Hristov, N. Kari, A. Jerković and Savić S., "Application of a CFD Model in Determination of the Muzzle Blase Overpressure in Small Arms and Its Validation by Measurement", *Tehnicki Vjesnik*, Vol. 15 May 2018, pp. 1399-1407, pp. 36-44.

[3] Chaturvedi E. and Dwivedi, R.K., "Computer aided design and analysis of a tunable muzzle brake", *Defence Technology*, Elsevier, Jun 18, 2018, pp. 89-94.

[4] Fureby, C. and Troeng, C., "A Computational Study of Unsteady Gun Tube Flows", FOI-R–3663–SE, Mar. 2013.

[5] Trebiński, R. and Czyżewska, M., "Estimation of the Increase in Projectile Velocity in the Intermediate Ballistics Period", *Central European Journal of Energetic Materials*, 2015, pp. 63-76.

[6] Zhao, X. and Lu, Y., "S Comprehensive Performance Evaluation Method Targeting Efficiency and Noise for Muzzle Brakes Based on Numerical Simulation", *Energies*, Vol. 15, May 22, 2022, 3576.

[7] Ahmed, N.Z., Jerković, D.D., Hristov, N.P. and Abaci, W.B., "Analytical and Experimental Investigation of the Muzzle Brake Efficiency", Facta Universitatis, Series: Mechanical Engineering, [S.l.], Jun 2022.

[8] Bougamre, A. and Huilin, L., "Multiphase CFD Simulation of Solid Propellant Combustion in a Small Gun Chamber", *International Journal of Chemical Engineering*, Vol. 0214 Hindawi Publishing Corporation.

[9] Olsson, S., Parmhed, O. and Wikström,N., "Projection 2015 Modeling and Experiments", FOI Swedish Defence Research Agency, FOI-R–4170–SE, Oct. 2015.

[10] Ingvarsson, M., Nordin-Bates, K., Olsson, S., Parmhed, O. and Wikström,N., "Methods for measuring recoil and modeling of internal and transitional ballistics processes", FOI Swedish Defence Research Agency, FOI-R–4461–SE, Nov. 2017.

[11] Cronemberger, P.O., Júnior, E.P. Lima, Gois, J.A.M. and Caldeira, A.B., "Theoretical and Experimental Study of the Interior Ballistics of a Rifle 7.62", *Engenharia Termica* (Thermal Engineering), Vol. 13, No. 2, Dec . 2014, pp. 20-27.

[12] Akçay, M. "Internal and Transitional Ballistic Solution for Spherical and Perforeted Propellants and Verification with Experimental Results", *Journal of Thermal and Technology*, April 2017.

[13] Hall, M.J. "Measuring felt recoil of sporting arms", *International Journal of Impact Engineering*, Vol. 35, Elsevier, 2008 pp.540-548.

[14] Canfield-Hershkowitz, B., Foster, T. and Meijer, W., "Rifle and Shotgun Recoil Test System", Senior Project, California Polytechnic State University, Dec. 2013.

[15] Lonzi, F., Martarelli, M. Santolini, C. and Scalise, L., "Measurement of firing impulse forces", *Proceedings of ISMA*, 2014, pp. 2065-2075.

[16] Court, F., "Case Study: enDAQ Sensor Firearms Testing", https://blog.endaq.com/slam-stick-x-rifle-test-blog-post.

[17] Higgins, E., https://blog.ammolytics.com/2019-01-01/project-cheap-rifle-accelerometer.html.

[18] SAAMI Gun Recoil, https://saami.org/wp-content/uploads/2022/11/Gun-Recoil-Formulae-2018-07-9.pdf.

[19] Carlucci, D.E. and Jacobson S.S., *Ballistics Theory and Design of Guns and Ammunition*, Third Edition, CRC Press, 2018.

[20] 4AW, https://4aw-store.myshopify.com/collections/muzzle-brakes/products/4aw-muzzle-brake-3-port.

[21] SilencerCo ., https://silencerco.com/shop/asr-muzzle-brake/.

[22] The OpenFOAM Foundation, https://openfoam.org/.

[23] High Speed Aerodynamic (HiSA) solver, Aeronautic Systems Competency Area of the Council for Scientific and Industrial Researchhttps://hisa.gitlab.io/

[24] FreeCAD, 3D parameteric modeler, https://www.freecad.org/

[25] White, F., *Fluid Mechanics* 7th Edition, McGraw-Hill, 2011.